Supporting Information

Porous VN nanosheet arrays on MXene carbon fibers for flexible supercapacitors

Deyang Zhang ‡*[a], Di Wang ‡[a], Binhe Feng [a], Jinbing Cheng *[b], Hailong Yan [b], Jin Chang [a, c], Zhaorui Wang [a], Paul K. Chu [d], Yongsong Luo *[a, b]

[a] *Henan Joint International Research Laboratory of New Energy Storage Technology, Xinyang Normal University, Xinyang 464000, P. R. China*

[b] *College of Physics and Electronic Engineering, Nanyang Normal University, Nanyang 473061, P. R. China*

[c] *Pingdingshan University, Pingdingshan 467000, P. R. China*

[d] *Department of Physics, Department of Materials Science & Engineering, and Department of Biomedical Engineering, City University of Hong Kong, Tat Chee Avenue, Kowloon, Hong Kong, China*

‡ *These authors contributed equally to this work.*

* Corresponding authors: zdy@xynu.edu.cn (D. Y. Zhang); chengjinbing1988@163.com (J. B.

Cheng); ysluo@xynu.edu.cn (Y. S. Luo)

Experimental section

1. Chemicals

The Ti_3AlC_2 powder (400 mesh) was purchased from Enwang New Materials Technology Co., Ltd., and N, N-dimethyl formamide (DMF, 99.9%) and polyacrylonitrile (PAN, MW = 150,000) were bought from Aladdin. Hydrofluoric acid (HF), Lithium fluoride (LiF), Ti_3AlC_2, melamine($C_3H_6N_6$), cobalt nitrate hexahydrate (Co $(NO_3)_2.6H_2O$), metavanadate (NH_4VO_3), oxalic acid ($C_2H_2O_4$), hexamethylene-tetramine ($C_6H_{12}N_4$), urea (CH_4N_2O), and ammonium fluoride (NH_4F) were analytical grade and all the chemicals were used without purification.

2. Synthesis of $Ti_3C_2T_x$.

$Ti_3C_2T_x$ MXene was synthesized by the minimally intensive layer delamination (MILD) method. MXene nanoflakes with large lateral sizes and few defects were produced. A mixture of HCl (12 M) and LiF was used to etch the raw Ti_3AlC_2. In detail, LiF (2 g) was added to 9 M HCl (40 mL) in a Teflon container (50 mL), and Ti_3AlC_2 (1 g) was added and stirred at 550 pm for 24 h at 35 °C. The powder was washed repeatedly with deionized water and centrifuged at 3,500 rpm for 5 min until the supernatant reached a pH of 6. Deionized water (10 mL) was added to the $Ti_3C_2T_x$ sediment, and after shaking vigorously for 5 min, the sediment swelled and delaminated into nanosheets, forming the concentrated aqueous ink. The dispersion

was centrifuged at 1,500 rpm for 30 min to obtain a dark-green supernatant of the $Ti_3C_2T_x$ colloidal solution. The supernatant was stored in hermetically sealed Arfilled bottles and refrigerated.

3. Preparation of MXCF

MXCF was synthesized by electrospinning, pre-oxidation, and carbonization. Polyacrylonitrile (0.65 g) was dispersed in 5 ml of the $Ti_3C_2T_x$ solution and stirred continuously for 6 h. The solution was placed in a 5 mL plastic syringe with an 18 G blunt-tip needle. A positive voltage (20 kV) was applied to the needle tip. The copper collector roller covered with an aluminum foil was grounded. The distance between the needle tip and collector was 12 cm, and the infusion rate of the solution was controlled to be 0.8 mL h^{-1}. The samples were electrospun at a relative humidity below 30%. The electrospun mats were stabilized in air at 267 ℃ for 2 h at a ramping rate of 3 ℃ min^{-1} and then carbonized under argon at a ramping rate of 2 ℃ min^{-1} at 800 ℃ for up to 2 h.

4. Preparation of MXCF@VN

In the typical fabrication process, 0.39 g of NH_4VO_3, 0.84 g of oxalic acid, and 0.05 g of hexamethylene-tetramine were dissolved in 44 ml of DI water and transferred to a 50-ml Teflon-lined autoclave. A piece of MXCF (1×1 cm^2) was immersed in the precursor solution in the autoclave. The autoclave was heated to 150 °C and kept for 0.5 h in the constant-temperature oven. After cooling down to

room temperature inside the oven, the carbon cloth was taken out, washed, and dried at 50 °C for 1 h. Finally, MXCF@VO_x placed downstream and urea (0.5 g) placed upstream were heated to 650 °C for 2 h under argon. CF@VN was prepared by the same method.

5. Preparation of Co_3O_4 on the Neural Network Substrate

Nanostructured Co_3O_4 was prepared on a neural network by a binder-free hydrothermal technique. Prior to the synthesis, the neural network was cleaned ultrasonically with HCL for 30 min, rinsed with DI water and ethanol successively, and dried at 60 °C for 8 h. In the typical synthesis, 1.164 g of Co $(NO_3)_2.6H_2O$), 0.28 g of NH_4F, and 1.2 g of CH_4N_2O were dissolved in 110 mL of DI water under stirring for 20 min at room temperature. The mixture was transferred to a Teflon-lined stainless-steel autoclave with the pretreated neural network placed vertically in the solution, placed in an oven, and then heated to 120 °C for 6 h. After removal from the autoclave, it was rinsed several times with DI water and ethanol, dried at 70 °C for 12 h, and calcinated in air at 350 °C for 30 min.

6. All-solid-state asymmetric supercapacitor

The flexible all-solid-state capacitor was assembled with MXCF@VN and Co_3O_4/NF as the positive and negative electrodes, respectively and 3 M KOH/PVA gel as the electrolyte. The polyvinyl alcohol (PVA) powder (2 g) was dissolved in 20 mL of DI water and heated to 90 ℃ under stirring until the solution became clear.

Subsequently, KOH (10 mL, 0.1 g mL^{-1}) was added dropwise to the solution and stirred. The KOH/PVA gel solution was coated between the electrodes (MXCF@VN and Co_3O_4/NF). After drying at room temperature for 1 h to solidify the gel, the firm all-solid-state ASC was obtained.

7. Materials characterization

The crystalline structure and phase of the samples were identified by X-ray diffraction (XRD, Bruker D2 PHASER) using Cu K_α (λ = 1.5418 Å) radiation at 40 kV and 40 mA and 2θ between 5° and 80° at room temperature. Raman spectroscopy was carried out on the INVIA Raman microprobe (Renishaw Instruments) with a 532 nm laser, 50× objective lens, and laser power of 5%. The chemical composition and states were analyzed by X-ray photoelectron spectroscopy (XPS, K-ALPHA 0.5 eV, monochromatic Al X-ray source) with a resolution of 0.3-0.5 eV. The sample morphology was examined by field-emission scanning electron microscopy (SEM, Hitachi S-4800) and transmission electron microscopy (TEM, FEI Tecnai G2 F20). Elemental analysis was performed by energy-dispersive X-ray spectroscopy (EDS, Bruker QUANTAX) on the TEM.

8. Electrochemical measurements

The electrochemical properties of CF@VN@ $Ti_3C_2T_x$ were determined in 3 M KOH on the CHI660E electrochemical workstation using the traditional three-electrode configuration at 25 °C with platinum and Hg/HgO as the counter and

reference electrodes, respectively. Cyclic voltammetry (CV) and galvanostatic charging-discharging (GCD) were performed at various scanning rates to gauge the rate capability of the active electrode. Electrochemical impedance spectroscopy (EIS) was conducted in a frequency region of 100 kHz to 0.01 Hz at an open circuit potential of 10 mV. The specific capacitance (C_m, F g^{-1}) was calculated by Eq. (1):

$$C_m = \frac{I \times \Delta t}{m \times \Delta V}, \quad (1)$$

where I (A) is the applied current, Δt(s) is the discharging time, ΔV (V) is the dischar ging potential range, and m (g) is the total mass of active materials, respectively. The theoretical pseudocapacitance was calculated by Eq. (2):

$$C = \frac{n \times F}{M \times V}, \quad (2)$$

where n (mol) is the number of electrons transferred in the redox reaction, M (g. mol^{-1}) is the molar mass of the materials, F (C. mol^{-1}) is Faraday's constant, and V (V) is the operating voltage window, respectively.

The asymmetric supercapacitor was assembled with Co3O4/NF as the positive electrode and CF@VN@ $Ti_3C_2T_x$ as the negative electrode. In order to obtain the best electrochemical characteristics of Co_3O_4// MXCF@VN, the charge balance between the two electrodes follows the relationship of q+ = q-, where q is the charge stored by the electrode calculated by Eq. (3):

$$q = C_m \times \Delta E \times m, \quad (3)$$

where Cm (F g^{-1}) is the specific capacitance, ΔE (V) is the potential range of the charging/discharging process, and m (g) is the mass loading of the active materials.

According to Eq. (3), the ideal mass ratio of the active materials on the positive electrode (MXCF@VN) to that on the negative electrode (Co_3O_4) (m^+/m^-) can be calculated by Eq. (4):

$$\frac{m_+}{m_-} = \frac{\Delta E_- \times C_-}{\Delta E_+ \times C_+} \quad (4)$$

The energy density (E) and power density (P) can be calculated by Eqs. (5) and (6):

$$E = \frac{1}{2} C_m (\Delta V)^2 \quad (5)$$

and

$$P = \frac{E}{\Delta t}, \quad (6)$$

where E (Wh kg^{-1}) is the energy density, m (F g^{-1}) is the specific capacitance, ΔV (V) is the operating potential window, P (kW kg^{-1}) is the power density, and Δt(s) is the discharging time.

To analyze the reaction kinetics, CV curves were acquired at different scan rates and the b values were derived according to the power law relationship between the redox peak currents and scanning rates:

$$i = aV^b, \quad (7)$$

where i is the peak current (mA), ν is the sweeping rate (mV s^{-1}), and a and b are variables. A b value of 0.5 or 1 represents the diffusion- or capacitive-controlled behavior, respectively.

$$(V) = k_1 V + k_2 V^{1/2} . \quad (8)$$

The first term on the right side of Eq. (8) corresponds to the capacitance-controlled effect and the other involves diffusion-controlled insertion. i(V) and v are the current at potential V, and the scanning rate, slope, and intercept are obtained by

plotting $i(V)/v^{1/2}$ against $v^{1/2}$.

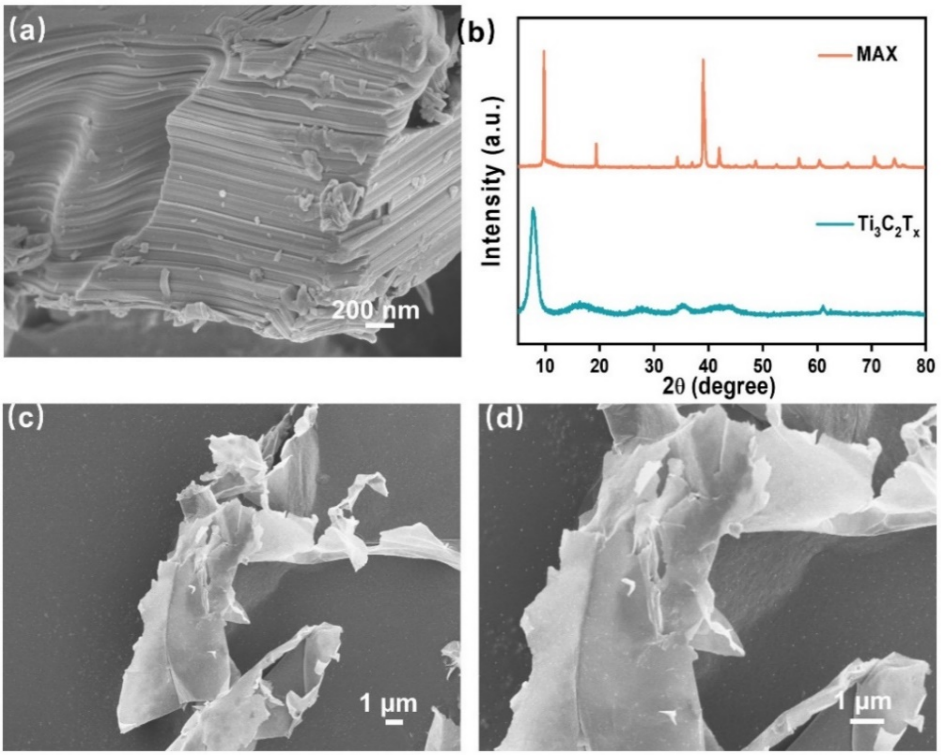

Fig. S1. (a) SEM images of MAX; (b) XRD spectra of MAX and $Ti_3C_2T_X$ and (c, d) SEM images of $Ti_3C_2T_X$.

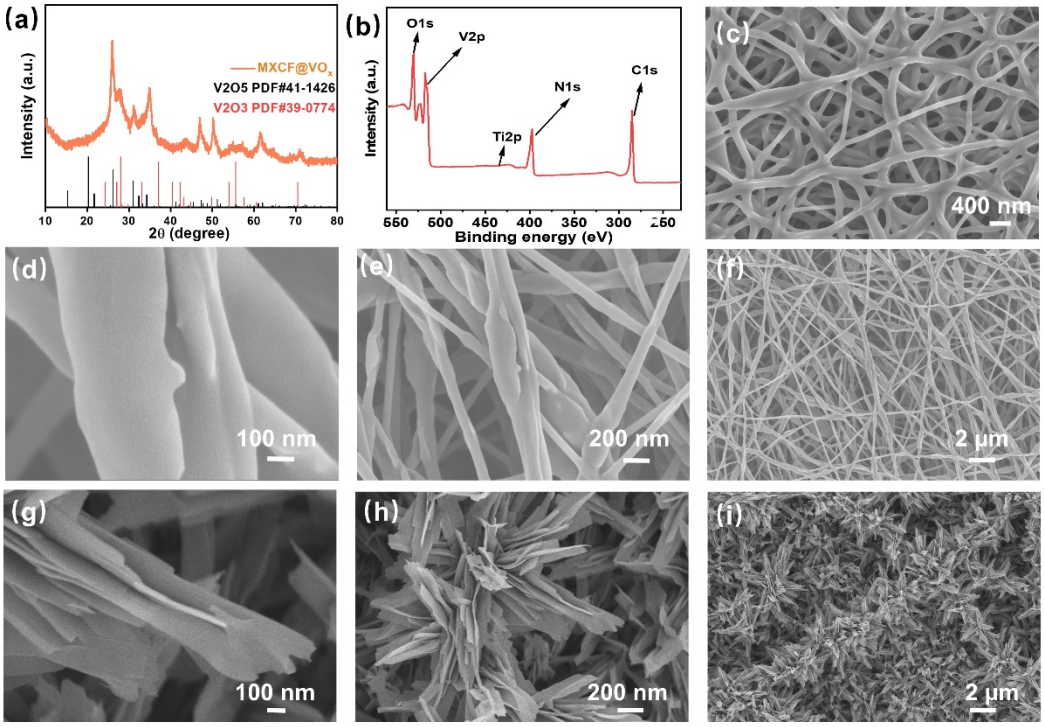

Fig.S2. (a) XRD spectra of MXCF@VO_x; (b) XPS survey spectra of MXCF@VN; (c) SEM images of CNF; (d-f) SEM images of MXCF and (g-i) SEM images of MXCF@VO_x.

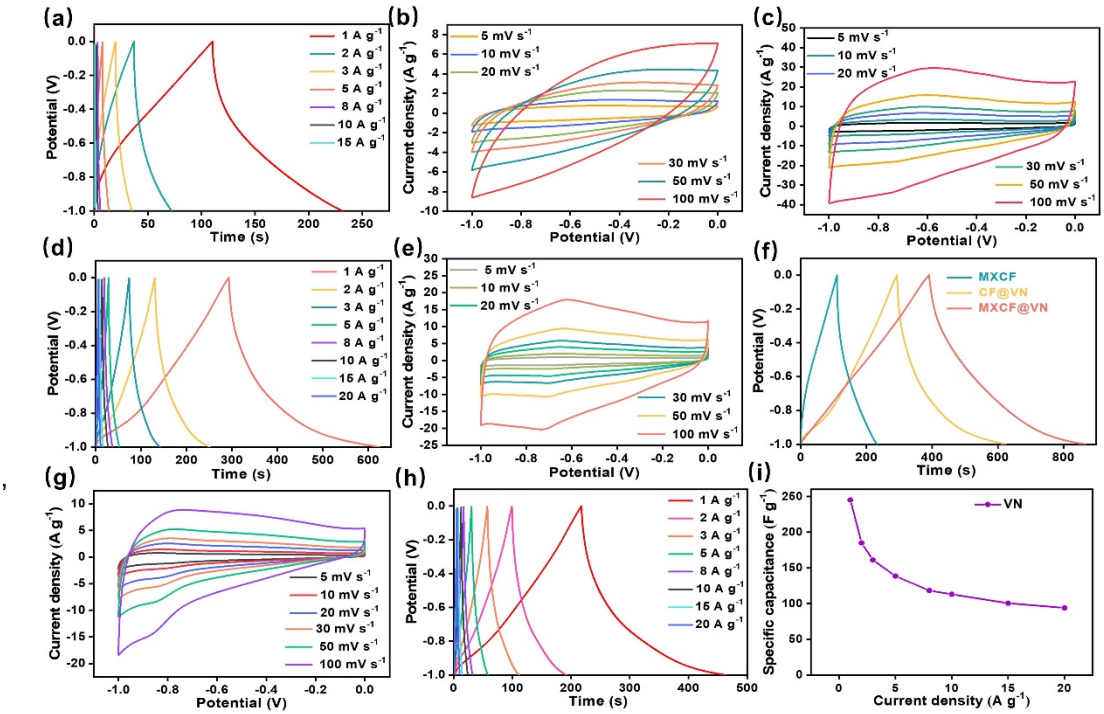

Fig. S3. (a) GCD and (b) CV curves of the MXCF electrolyte at various scanning rates (5–100 mV s^{-1}) and current densities (1–15 A g^{-1}); (c) CV curves of the electrolyte of MXCF@VN at various scanning rates (5–100 mV s^{-1}); (d) GCD and (e) CV curves of the CF@VN electrolyte at various scanning rates (5–100 mV s^{-1}) and current densities (1–20 A g^{-1}); (f) Comparison of the GCD curves of the electrolyte of MXCF@VN, CF@VN, and MXCF at a current density of 1 A g^{-1}; (g) CV and (h) GCD curves of the VN electrolyte at various scanning rates (5–100 mV s^{-1}) and current densities (1–20 A g^{-1}) and (i) Specific capacities at different current densities.

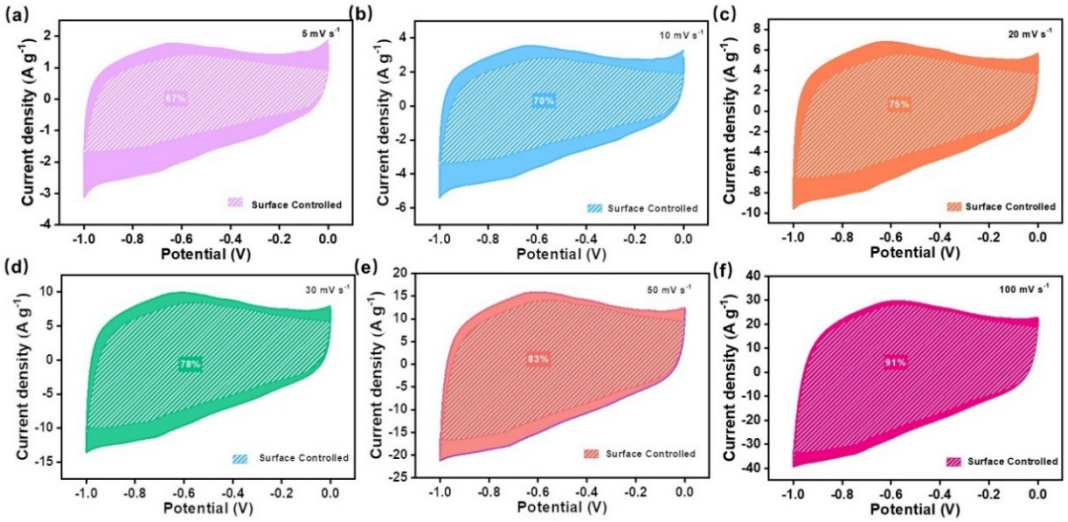

Fig. S4. (a-f) Capacitive contributions at a scanning rate of 5-100 mV s^{-1}.

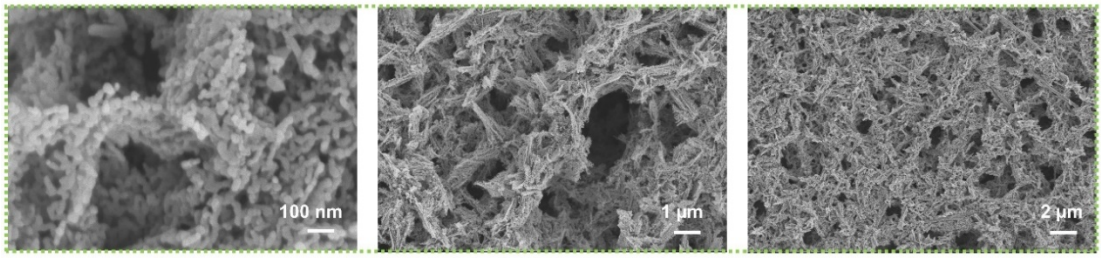

Fig.S5. SEM images after 10,000 cycles.

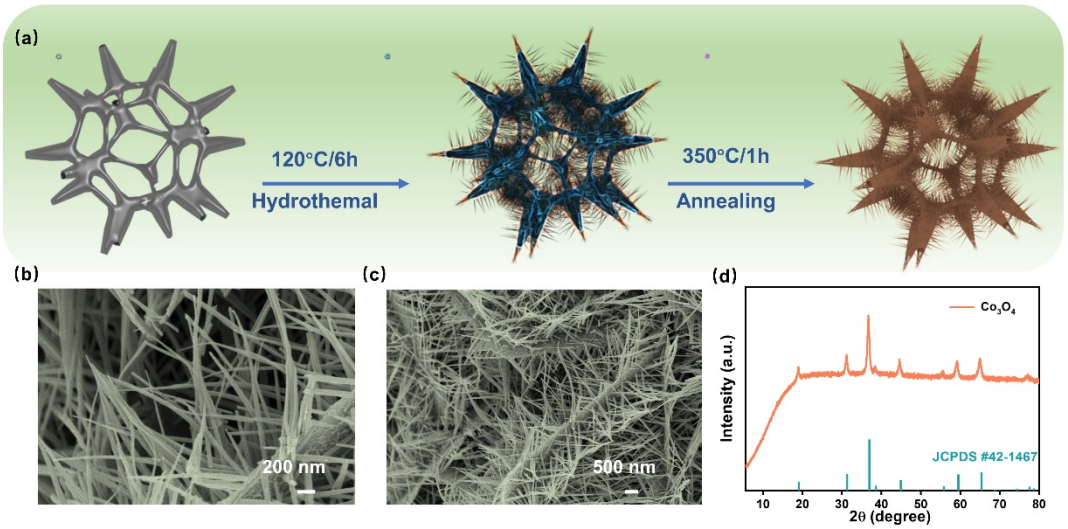

Fig. 6. (a) Schematic illustration of the processing of porous Co_3O_4 electrodes; (b, c) SEM images of Co_3O_4; (d) XRD patterns.

Co_3O_4 is a promising cathode material for ASCs because of its high theoretical specific capacitance, environmental friendliness, simple synthesis and low cost[1,2]. However, due to the low conductivity of the material, the specific capacitance is small, which limits the use of flexible ASC. In this regard, an effective method is to directly grow Co_3O_4 nanostructures on a highly conductive substrate, so we chose a nickel mesh as a base. In addition, another reason for choosing Co_3O_4 as the positive electrode is to refer to the previous research. For example, Sun[3] et al. used Co_3O_4 NMAs as the positive electrode and VN NMAs as the negative electrode. At a current density of 1.0 A cm^{-3}, the device has a high energy density of 13.2 mWh cm^{-3}.

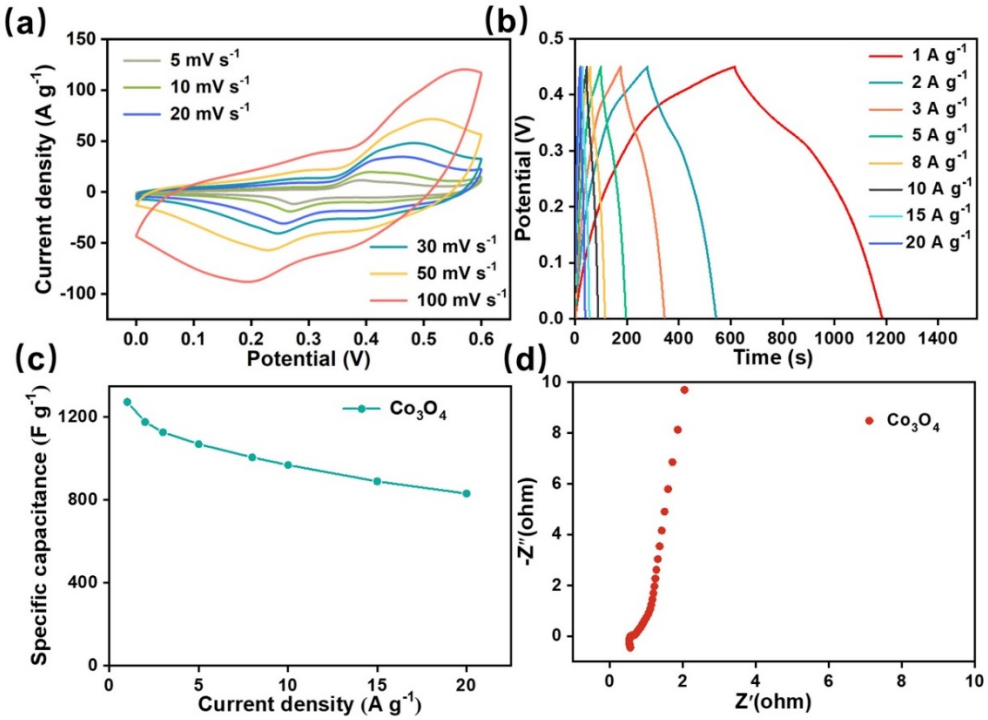

Fig. S7. Electrochemical evaluation of the Co_3O_4 electrode in the three-electrode system in the 3 M KOH aqueous electrolyte: (a) CV curves at various scanning rates (5–100 mV s^{-1}), (b) GCD curves at various current densities (1–20 A g^{-1}), (c) Specific capacities at different current densities and (d) Nyquist plot.

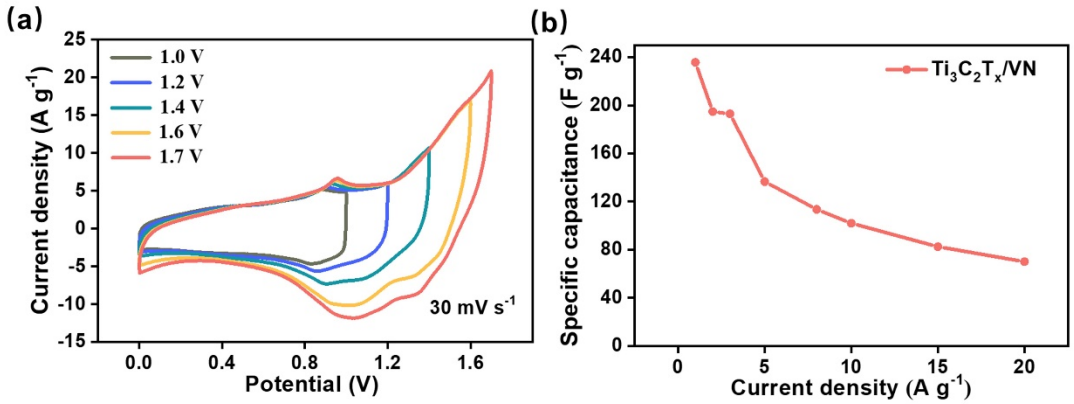

Fig. S8. (a) CV curves in different potential voltage windows and (b) Specific capacitances at different current densities.

Table S1. Specific capacities of different electrode materials at different current densities.

Current density	Specific capacitance (F g^{-1})			
(A g^{-1})	MXCF@VN	CF@VN	MXCF	VN
1	476.7	331.4	120.7	245.2
2	368	242.2	70	185
3	327	204.9	45	161.1
8	254.4	141.6	19.2	138.4
10	241	130	14	118.4
15	220.5	112.5	10	113
20	206	102	/	94

Table S2. Comparison of the electrochemical properties of different electrodes based on MXCF@VN.

Materials	Specific capacitance ($F\ g^{-1}$)	ΔV	Cycle number	Capacitance retention (%)	Test current ($A\ g^{-1}$)	Reference
MXCF@VN	476.7	1	10,000	98.5	20	This Work
VN/C	195.7	1.2	5000	75	5	Ref [4]
VNQD/CNF	380	1	10,000	90	10	Ref [5]
VN/C	385	1.2	10,000	88.9	2	Ref [6]
Mesoporous VN	450	1.1	5000	83	10	Ref [7]
VN/NG	370	1.2	10,000	98.66	10	Ref [8]
$Ti_3C_2T_x$ /VN	382.1	1	5000	93.5	15	Ref [9]
VN/PEDOT	226.2	1	5000	91.5%	10	Ref [10]
VN/NCS	148	1	5000	98.5	20	Ref [11]
VN/NCNT/NCN	232.9	1	5000	91	10	Ref [12]
MXene/CNT	550	0.8	5000	98	20	Ref [13]
$Ti_3C_2T_x$	426	0.6	10,000	92	8	Ref [14]

Table S3. Areal energy and power densities of the Co_3O_4/NF//MXCF@VN ASC.

Current density ($A\ g^{-1}$)	Power density ($KW\ kg^{-1}$)	Energy density ($Wh\ kg^{-1}$)
1	0.801	83.95
2	1.602	69.35
3	2.404	68.71
5	4.006	48.63
8	6.408	40.41
10	8.020	36.32
15	12.015	29.37
20	16.020	24.92

Table S4. Areal energy and power densities of the Co_3O_4/NF//MXCF@VN ASC and previously reported high-performance supercapacitors.

Materials	Potential window (V)	Energy densities (Wh kg^{-1})	Power densities (W kg^{-1})	References
Co_3O_4//$Ti_3C_2T_x$/VN	(0-1.6)	83.95	800	This Work
VN@C//AC	(0-1.5)	17.3	701.57	Ref [15]
NCA//VN/PEDOT	(0-1.6)	48.36	1600	Ref [16]
MnO2@CC//VN-NWs@CC	(0.5-1.6)	57.9	261.5	Ref [17]
NiO/rGO//VNNW/NG	(0-1.6)	20.2	850	Ref [18]
PCNS@VNNP//NiO	(0-1.6)	47.2	800	Ref [19]
VNQD/PC//Ni $(OH)_2$	(0-1.6)	31.2	780	Ref [20]
HPCF@VNNP//Ni $(OH)_2$	(0-1.6)	39.3	400	Ref [21]
V_2O_3/C//VN/NCS	(0-1.6)	19.8	800	Ref [22]
0.04-VN/NCS-2//$NiCo_2S_4$	(0-1.6)	21	800	Ref [23]

Materials	Potential window (V)	Energy densities mWh cm^{-2}	Power densities mW cm^{-2}	References

Fe_2O_3@VN/CC//RuO_2/CC	0-1.4V	0.5	12.28	Ref [24]
ZNCO/NF//VN/CC	0-1.6V	0.185	22.4	Ref [25]
VN/NPC// VN/NPC SSC	0-1V	21.97	0.5	Ref [26]

References

[1] T. Zhu, J. S. Chen and X. W. Lou, Journal of Materials Chemistry A, 2023, 11, 23087-23087.

[2] H. Zhou, Y. Sun, H. Yang, Y. Tang, Y. Lu, Z. Zhou, S. Cao, S. Zhang, S. Chen, Y. Zhang and H. Pang, Advanced Science, 2023, 10.

[3] J. Sun, P. Man, Q. Zhang, B. He, Z. Zhou, C. Li, X. Wang, J. Guo, J. Zhao, L. Xie, Q. Li, J. Sun, G. Hong and Y. Yao, Applied Surface Science, 2018, 447, 795-801.

[4] Liu, Y.; Liu, L.; Tan, Y.; Kong, L.; Kang, L.; Ran, F., Well-dispersed vanadium nitride on porous carbon networks derived from block copolymer of PAN-b-PDMC-b-PAN absorbed with ammonium metavanadate for energy storage application. The Journal of Physical Chemistry C 2017, 122 (1), 143-149.

[5] Wu, Y.; Ran, F., Vanadium nitride quantum dot/nitrogen-doped microporous carbon nanofibers electrode for high-performance supercapacitors. Journal of Power Sources 2017, 344, 1-10.

[6] Q. Sun, Y. Lv, X. Wu, W. Jia, J. Guo, F. Tong, D. Jia, Z. Sun, X. Wang, Hydrothermal synthesis of coralloid-like vanadium nitride/carbon nanocomposites for high-performance and long-life supercapacitors, J. Alloys Compd. 818 (2020) 152895.

[7] Lee, H.-M.; Jeong, G. H.; Kim, S.-W.; Kim, C.-K., Low-temperature direct synthesis of mesoporous vanadium nitrides for electrochemical capacitors. Applied Surface Science 2017, 400, 194-199.

[8] Balamurugan, J.; Karthikeyan, G.; Thanh, T. D.; Kim, N. H.; Lee, J. H., Facile synthesis of vanadium nitride/nitrogen-doped graphene composite as stable high performance anode materials for supercapacitors. Journal of Power Sources 2016, 308, 149-157.

[9] Ti3C2Tx/VN

[10] Chen, M. H., Fan, H., Zhang, Y., Liang, X. Q., Chen, Q. Q., Xia, X. H., Coupling PEDOT on Mesoporous Vanadium Nitride Arrays for Advanced Flexible All-Solid-State Supercapacitors. Small 2020, 16, 2003434.

[11] X. Jiang, W. Lu, X. Yu, S. Song, Y. Xing, Fabrication of a vanadium nitride/N-doped carbon hollow nanosphere composite as an efficient electrode material for asymmetric supercapacitors, Nanoscale Adv 2(9) (2020) 3865-3871.

[12] J. Liu, X. He, F. Guo, B. Liu, Z. Sun, L. Zhang, H. Chang, Vanadium nitride nanoparticle decorated N-doped carbon nanotube/N-doped carbon nanosheet hybrids via a C3N4 self-sacrificing method for electrochemical capacitors, RSC Advances 12(24) (2022) 15354-15360.

[13] H. Xu, J. Fan, H. Su, C. Liu, G. Chen, Y. Dall'Agnese, Y. Gao, Metal Ion-Induced Porous MXene for All-Solid-State Flexible Supercapacitors, Nano Lett. 23 (2023) 283.

[14] X. Liu, Y. Liu, S. Dong, X. Zhang, L. Lv, S. He, Room-temperature prepared MXene foam via chemical foaming methods for high-capacity supercapacitors, J. Alloys Compd. 945 (2023).

[15] M.R. Pallavolu, Y. Anil Kumar, R.R. Nallapureddy, H.R. Goli, A. Narayan

Banerjee, S.W. Joo, In-situ design of porous vanadium nitride@carbon nanobelts: A promising material for high-performance asymmetric supercapacitors, Applied Surface Science 575 (2022) 151734.

[16] Chen, M. H., Fan, H., Zhang, Y., Liang, X. Q., Chen, Q. Q., Xia, X. H., Coupling PEDOT on Mesoporous Vanadium Nitride Arrays for Advanced Flexible All-Solid-State Supercapacitors. Small 2020, 16, 2003434.

[17] M. Ma, Z. Shi, Y. Li, Y. Yang, Y. Zhang, Y. Wu, H. Zhao, E. Xie, High-performance 3 V “water in salt” aqueous asymmetric supercapacitors based on VN nanowire electrodes, J. Mater. Chem. A 8(9) (2020) 4827-4835.

[18] T.S. Lim, I.W. Ock, J. Lee, S.G. Jo, Y.W. Jung, S.-H. Kwon, T. Song, W.I. Park, J.W. Lee, Freestanding vanadium nitride nanowire/nitrogen-doped graphene paper with hierarchical pore structure for asymmetric supercapacitor anode, J. Alloys Compd. 934 (2023) 167858.

[19] G. Wang, S. Hou, C. Yan, X. Zhang, W. Dong, Preparation of three-dimensional vanadium nitride porous nanoribbon/graphene composite as an efficient electrode material for supercapacitors, *J. Mater. Sci. Mater. Electron.* 29(15) (2018) 13118-13124.

[20] Y. Yang, K. Shen, Y. Liu, Y. Tan, X. Zhao, J. Wu, X. Niu, F. Ran, Novel Hybrid Nanoparticles of Vanadium Nitride/Porous Carbon as an Anode Material for Symmetrical Supercapacitor, Nano-Micro Lett. 9(1) (2016) 6.

[21] Y. Liu, L. Liu, Y. Tan, L. Kong, L. Kang, F. Ran, Well-Dispersed Vanadium Nitride on Porous Carbon Networks Derived from Block Copolymer of PAN-b-

PDMC-b-PAN Absorbed with Ammonium Metavanadate for Energy Storage Application, *J. Phys. Chem. C*. 122(1) (2018) 143-149.

[22] X. Jiang, W. Lu, X. Yu, S. Song, Y. Xing, Fabrication of a vanadium nitride/N-doped carbon hollow nanosphere composite as an efficient electrode material for asymmetric supercapacitors, *Nanoscale Adv.* 2(9) (2020) 3865-3871.

[23] X. Jiang, W. Lu, Y. Li, Y. Yu, X. Zhou, X. Liu, Y. Xing, An Eco-Friendly Nitrogen Source for the Preparation of Vanadium Nitride/Nitrogen-Doped Carbon Nanocomposites for Supercapacitors, ChemElectroChem 6(13) (2019) 3445-3453.

[24] H. Zhou, M. Alam, Y. Wu, Y. Zeng, A.N. Gandi, J. Zheng, W. Zhu, Z. Wang, H. Liang, Synergy of VN and Fe2O3 Enables High Performance Anodes for Asymmetric Supercapacitors, ACS Applied Materials & Interfaces 15(15) (2023) 18819-18827.

[25] Z. Wu, H. Li, H. Li, B. Yang, R. Wei, X. Zhu, X. Zhu, Y. Sun, Direct growth of porous vanadium nitride on carbon cloth with commercial-level mass loading for solid-state supercapacitors, Chemical Engineering Journal 444 (2022).

[26] Z. Wu, Q. Chen, C. Li, L. Zhu, Y. Huang, X. Zhu, X. Zhu, Y. Sun, Hydrogel-derived nitrogen-doped porous carbon framework with vanadium nitride decoration for supercapacitors with superior cycling performance, Journal of Materials Science & Technology 155 (2023) 167-174.